A 0-dimensional cavity growth submodel for use in reactor models of underground coal gasification

Greg Perkins[1,2]

Abstract Modelling of the underground coal gasification process is dependent upon a range of sub-models. One of the most important is the calculation of the cavity growth rate as a function of various operating conditions and coal properties. While detailed 1-dimensional models of coal block gasification are available, it is not easy to couple them directly with reactor models, which aim to simulate the complete process. In this paper, a 0-dimensional cavity growth sub-model is presented. The model is based on the concept of a surface reaction and incorporates physics to account for moisture evaporation, water influx, coal pyrolysis, coal thermo-mechanical fragmentation and the build up of an ash layer on the char. The model is validated using measurements from laboratory experiments on coal cores and coal blocks. A comparison of calculated results from several UCG field trials shows that the model can provide good estimates of cavity growth rate for reasonable input parameters. Finally, simulation results of cavity growth in the combustion and gasification zones as a function of the bulk gas temperature, gas pressure, water influx rate, ash layer thickness and coal fragmentation behaviour are presented.

Keywords Underground coal gasification · Cavity growth · Chemical reaction

Nomenclature

A_k	Pre-exponential factor in rate of reaction k (1/s)
$[B]$	Inverse effective diffusion matrix
C_i	Concentration of species i (kmol/m^3)
$C_{p,g}$	Gas specific heat capacity (J/kg K)
$C_{p,s}$	Solid specific heat capacity (J/kg K)
d_{pore}	Pore diameter (m)
$[D]$	Diffusivity matrix
D_{eff}	Effective diffusivity (m^2/s)
D_K	Knudsen diffusivity (m^2/s)
D_{ij}	Binary diffusivity for species ith, jth pair (m^2/s)
D_{im}	Diffusivity of species i in mixture (m^2/s)
E_k	Activation energy for reaction k (kJ/mol)
F	Error function for mass balance (kg/m^2 s)
g	Error function for energy balance (kJ/m^2 s)
Gr	Grashof number
h	Heat transfer coefficient (W/m^2 K)
$h_{m,i}$	Mass transfer coefficient (m^2/s)
J_w^i	Gas diffusion flux (kg/m^2 s)
$J_{i,k}$	Entry i,k in Jacobian matrix
$k_{f,k}$	Forward rate for reaction k
L	Characteristic length (m)
n	Power law exponent, distance normal to surface
Nu	Nusselt number
N_g	Number of gas species
N_R	Number of reactions
P_g	Gas pressure (Pa)
Pr	Prandtl number, $\text{Pr} = C_{p,g}\mu_g/\lambda_g$
q_w	Subsurface heat flux (kJ/m^2 s)
r_k	Rate of reaction k (kmol/m^2 s)
$\mathbb{R}$	Gas constant (=8.314 J/mol K)
Re	Reynolds number, $\text{Re} = \rho_g v_g L/\mu_g$

✉ Greg Perkins
greg.perkins@martinparry.com.au; g.perkins@uq.edu.au

1 Martin Parry Technology, Brisbane, QLD 4001, Australia

2 School of Chemical Engineering, The University of Queensland, Brisbane, QLD 4072, Australia

Sc	Schmidt number
Sh	Sherwood number
T_{amb}	Coal ambient temperature (K)
T_{dry}	Drying temperature (K)
T_f	Film temperature (K)
T_g	Gas temperature (K)
T_{vm}	Volatile matter release temperature (K)
T_w	Wall temperature (K)
v_c	Cavity growth rate (m/s, m/day)
W_i	Species molecular weight of species i (kg/kmol)
$\bar{W}$	Mean mixture molecular weight (kg/kmol)
X_c^{fc}	Coal fragmentation factor
X_g^i	Mole fraction of the ith species in bulk gas
X_w^i	Mole fraction of the ith species at wall
Y_f^i	Mass fraction of the ith species in gas film
Y_g^i	Mass fraction of the ith species in bulk gas
Y_w^i	Mass fraction of the ith species at wall
Y_{pr}^{fc}	Mass fraction of fixed carbon from proximate analysis
Y_{pr}^{vm}	Mass fraction of volatile matter from proximate analysis
Y_{pr}^w	Mass fraction of moisture from proximate analysis
Y_{pr}^{ash}	Mass fraction of ash from proximate analysis
α_k	Temperature exponent in rate of reaction k
β	Under-relaxation factor
δ_{AB}	Concentration boundary layer thickness (m)
δ_{ij}	Kroneker delta function
δ_T	Thermal boundary layer thickness (m)
ε	Emissivity
λ_g	Gas thermal conductivity (W/m K)
μ_g	Gas viscosity (Ns/m^2)
$v_{i,k}$	Stoichiometric coeff of species i in reaction k
ρ_g	Gas material density (kg/m^3)
ρ_w	Gas density at film conditions (kg/m^3)
ρ_s	Solid material density (kg/m^3)
σ	Stefan–Boltzmann constant
τ	Tortuosity ($=\sqrt{2}$)
ϕ_{ash}	Porosity of ash
ϕ_c	Porosity of coal
$\dot{\phi}_w^i$	Subsurface flux of the ith species (kg/m^2 s)
$\dot{\phi}_w^{vm,i}$	Volatiles flux of the ith species (kg/m^2 s)
$\dot{\phi}_l^{H_2O}$	Water influx rate (kg/m^2 s)
$\dot{\omega}_w^i$	Wall flux of the ith species (kg/m^2 s)
$\dot{\omega}_f^i$	Fragmented flux of the ith species (kg/m^2 s)
$\Delta H_{r,k}$	Heat of reaction for reaction k (kJ/kmol)
ΔH_{vap}	Latent heat of vaporisation for water (kJ/kg)

1 Introduction

In this paper, a 0-dimensional submodel for simulating the cavity growth process in underground coal gasification is described. The submodel is a relatively simple and numerically robust description of the gasification of coal. The presented model can be used as a standalone application or incorporated into reactor models of underground coal gasification built with reservoir, computational fluid dynamic or dynamic process simulators. This paper provides a review of previous work, describes the coal block gasification process, develops the mathematical basis for the 0-dimensional cavity growth submodel and compares results of the model with measured laboratory combustion experiments and estimates of cavity growth rates from several field trials. Finally, the submodel is used to investigate the effects of key operating conditions and coal properties on the rate of cavity growth in underground coal gasification.

Massaquoi and Riggs (1983) developed a 1-D numerical model of a drying and combusting wet coal slab and compared simulation results to laboratory combustion experiments of Texas lignites. Park and Edgar (1987) also developed a 1-D model which accounted for evaporation, pyrolysis and gasification of the char, plus the development of an ash layer on the char surface. Park and Edgar only considered oxidising conditions and found growth rates were controlled by mass transfer. Britten (1986) developed a computer model which assumed that the exposed coal underwent thermomechanical failure forming a packed bed of dried and pyrolysed char. More recently, Samdani et al. (2016a, b) presented a dynamic 1-D model for coal block gasification and coupled it to a CSTR model of the void space and a plug flow model of the rubble zone to forecast cavity growth in UCG . Perkins and Sahajwalla (2005) have presented a 1-dimensional model of coal block gasification that was validated through comparison with both measured data from laboratory experiments and observations from field trials. Simulations showed that cavity growth can be controlled by either mass transfer through the boundary layer or the heat transfer required to cause a breakdown of the coal material (Perkins and Sahajwalla 2006). The operating conditions which have the greatest impact on cavity growth rate were found to be: temperature, water influx, pressure and gas composition, while the important coal properties were: the coal fragmentation behaviour, coal composition and the thickness of the ash layer.

While, several 0-dimensional models of the gasification of coal have been developed, they are relatively simple and have not been separately validated. The channel model of van Batenburg (1992) incorporated a surface reaction

model between coal and the gases flowing through the underground reactor, while Kuyper used a similar surface reaction model when investigating the detailed fluid flow and transport phenomena in a UCG channel (1994).

Thermal reservoir simulators that use a porous medium approach can also be used to model UCG. Jiang et al. (2019) evaluated the beneficial impacts of undertaking UCG beneath heavy oil reservoirs, while Kasani and Chalaturnyk (2017) investigated the coupling of reservoir and geomechanical aspects in a CRIP-style UCG process. Seifi et al. (2011) compared the linear and parallel CRIP configurations of the UCG technology. The porous medium approach can capture most of the key phenomena, however the main disadvantage is that sub-grid scale processes are not resolved and heat and mass transfer in void spaces is not as sophisticated as in computational fluid dynamic simulators (Perkins 2018b). The issue of kinetic upscaling remains, and while such models can be history matched to field trial data, there are questions over the reliability of the models when extrapolating to new coal seams.

The development of a validated 0-dimensional model that could be embedded within reservoir and computational fluid dynamic models of the UCG process would be very useful. It is envisaged that such a model will have the advantages of being able to directly use kinetic data measured in the laboratory and represent local heat and mass transport phenomena in detail.

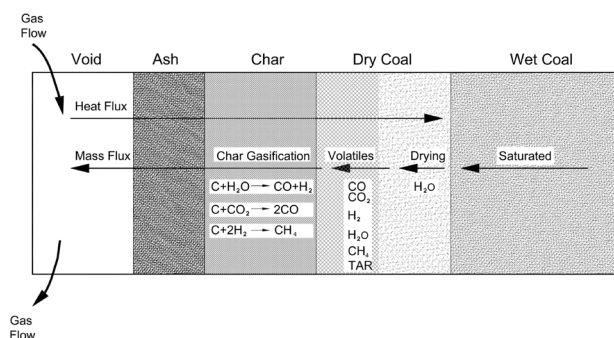## 2 Description of coal block gasification

Before proceeding to describe the submodel for cavity growth in detail, it is useful to develop an understanding of coal block gasification in underground coal gasification. A schematic of an underground coal gasifier is shown in Fig. 1. In its most general form, UCG consists of an injection well drilled from the surface through which an oxidant is injected into the coal seam after its ignition. A number of zones exist within the underground coal gasifier,
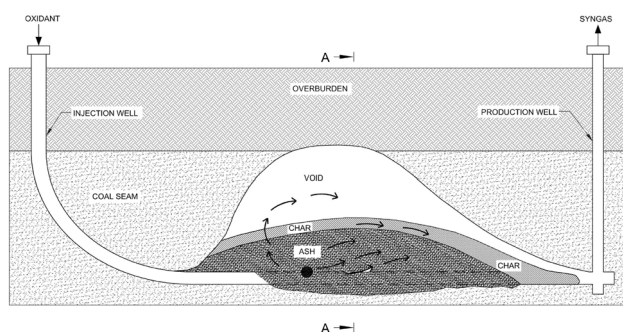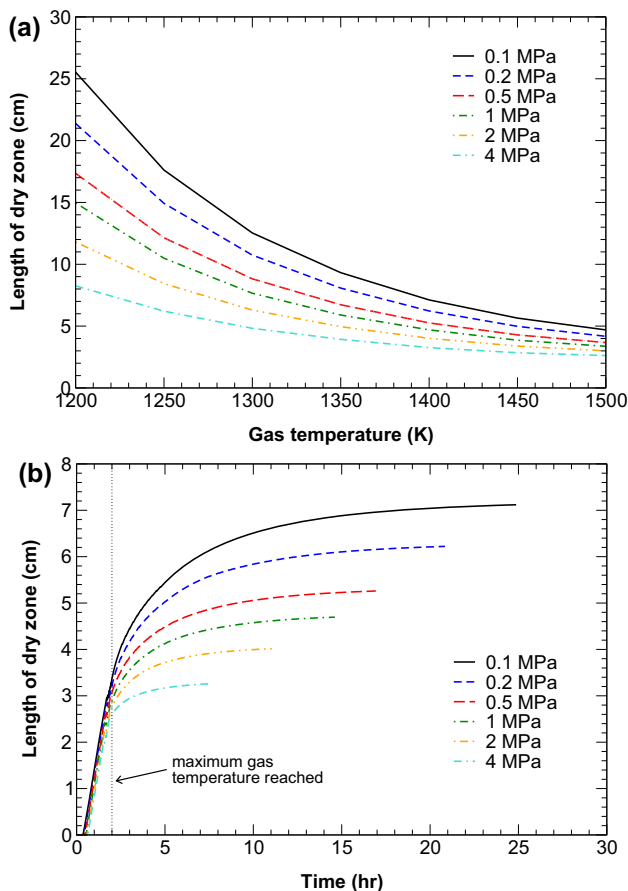
including a combustion zone in which temperatures may reach $\sim$ 2000 K, a gasification zone which is devoid of oxygen, and a low temperature pyrolysis and drying zone. The synthesis gas produced from these three zones is extracted via the production well and taken to the surface. Since many coal seams are saturated with water, the gasification process may occur inside a gas bubble located within the coal seam. Figure 2 shows a schematic of the coal block gasification processes that are of concern in this work. In the virgin coal seam, a positive water influx is assumed and a sharp evaporation front separates the wet coal from the dried coal. Volatiles are released ahead of the evaporation front forming a porous char which reacts with steam, CO_2 and hydrogen. An ash layer may form on the outside of the char inhibiting the transport of heat and mass. The coal block is exposed to the inside of the cavity, where the bulk gas temperature, composition and pressure are known.

The current work is focused on developing a suitable reduced model of the coal block gasification process. In order to guide this development, the model of Perkins and Sahajwalla (2005) has been used to investigate the characteristic time and length scales required to achieve a psuedo-steady-state in coal block gasification. Figure 3a, b show the simulation results obtained using a Surat basin coal for a range of gas temperatures and operating pressures. The calculated length of the dry zone as a function of bulk gas temperature and pressure is shown in Fig. 3a. It can be seen from this figure that at gas temperatures above 1300 K the dry zone length is 13 cm or less, and approaches 5 cm at all pressures as the gas temperature approaches 1500 K. These results show that the length scale over which coal is converted from its virgin state to gaseous products is on the order of a few centimetres, and to a good approximation the reaction of the coal can be considered to occur at a reaction front when compared to the length scales associated with a field scale operation (> 10 m). In Fig. 3b, the time taken to reach pseudo-steady-state for a range of pressures at a gas temperature of 1400 K are

Fig. 1 Schematic of an underground coal gasifier (from Perkins 2018a)

Fig. 2 A detailed schematic of coal block gasification in underground coal gasification (from Perkins 2018a)

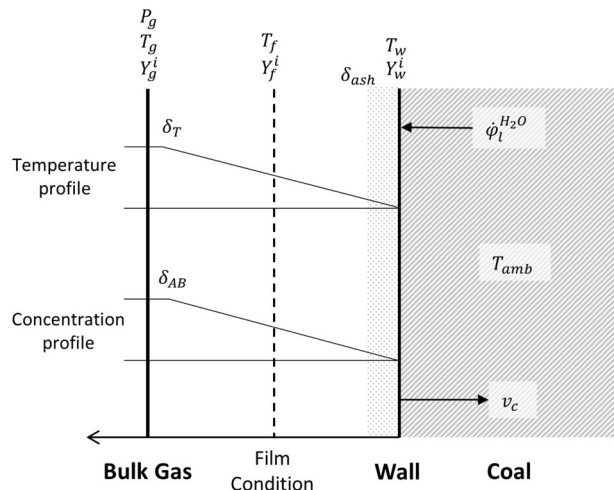Fig. 4 Schematic of the coal wall cavity growth model

wall. The rate of mass transfer is influenced by the concentration boundary layer thickness, δ_{AB} and the ash layer thickness, δ_{ash}, while the rate of heat transfer is influenced by the thermal boundary layer thickness, δ_T. The model accounts for direct chemical reaction of the coal and spalling of the coal due to thermo-mechanical breakage, in oxidizing and reducing atmospheres in the presence of multicomponent mass transfer. Away from the wall, the coal is at ambient temperature, T_{amb}, and a flux of liquid water, $\dot{\varphi}_l^{H_2O}$, may also be present. All reactions, including drying and devolatilisation of the coal are assumed to occur at the wall surface. In principle, the controlling mechanisms for cavity growth could be chemical kinetics at low temperature (regime I), combined chemical kinetics and mass transfer at moderate temperatures (regime II) or bulk diffusion control at high temperatures (regime III). In some circumstances the rate may be governed by heat transfer.

3.1 Chemical reactions

The chemical reaction between a solid carbon molecule (S) and reactant gas molecule (G) at the wall layer is given by:-

$$v_c S + v_g G \rightarrow products. \tag{1}$$

For simplicity char is taken to be pure carbon and reacts according to the following stoichiometry:

$$C + O_2 \xrightarrow{k_{f,1}} CO_2 \tag{2}$$

$$C + H_2O \xrightarrow{k_{f,2}} CO + H_2 \tag{3}$$

$$C + CO_2 \xrightarrow{k_{f,3}} 2\,CO \tag{4}$$

$$C + 2H_2 \xrightarrow{k_{f,4}} CH_4. \tag{5}$$

Fig. 3 The length of the dry zone in coal block gasification: **a** effect of gas temperature and pressure and **b** time to achieve steady-state cavity growth for a bulk gas temperature of $T_g = 1400\,K$

shown. Typically, psuedo-steady-state is reached within 10 h, however at high temperatures and pressures, the psuedo-steady-state condition can be achieved in just a few hours. In comparison to the time scales of a full scale operation, these results show that the cavity growth process can be considered to be pseudo-steady-state at all times.

3 The mathematical model

From the simulation results presented above it can be concluded that to a good approximation the chemical reaction of the coal can be modelled as a surface reaction on the exposed coal surface and that the rate of cavity growth can be assumed to be at pseudo-steady-state. Figure 4 shows a schematic of the proposed model, showing the wall layer, the bulk gas and the film condition between the two. The rate at which the coal is consumed, known as the cavity growth rate, v_c, is calculated by accounting for heat and mass transfer between the coal layer and the bulk gas and chemical reactions which occur at the surface of

The porous structure of the solid is assumed to be approximated by infinitely long pores extending from the surface into the solid. In effect, it is assumed that the solid is semi-infinite in extent away from the surface (van Batenburg 1992). In order to derive the appropriate rate expressions, we consider the conservation of mass equation, written in terms of concentration for a single infinitely long pore extending from the surface (eg. Levenspiel 1972). After some manipulation a relation for the reaction rate accounting for pore diffusion effects can be derived as:

$$r_k = \frac{\phi_c}{\tau} \sqrt{\frac{8 \left(\frac{v_g}{v_c}\right)\left(\frac{k_{f,k}}{W_c}\right) D_{eff,i}}{d_{pore}(n+1)}} [C_i]^{\frac{n+1}{2}}, \tag{6}$$

where ϕ_c is the porosity of the coal, n is the order of the reaction, d_{pore} is the diameter of the pore and $k_{f,k}$ is the intrinsic chemical reactivity of the char (kg-char/m^2 s-[kmol-reactant/m^3]^n) and is assumed to have an Arrhenius form given by $k_{f,k} = A_k T^{\alpha_k} \exp\left(-\frac{E_k}{RT}\right)$. The molecular weight of the char is represented by W_c and the effective diffusivity accounts for both molecular and Knudsen diffusion, using:

$$\frac{1}{D_{eff,i}} = \frac{1}{D_{K,i}} + \frac{1}{D_{im}}, \tag{7}$$

and

$$D_{K,i} = \frac{d_{pore}}{3} \sqrt{\frac{8000RT}{\pi W_i}}. \tag{8}$$

The intrinsic reactivity of char to H_2O and CO_2 is taken from the work of Roberts and Harris (2000) and uses a pressure order of $n = \frac{1}{2}$ based on correlated experimental measurements. The intrinsic reactivity of char to H_2 is taken to be first order based on the work of Tomita et al. (1977). It is recognised that the power law form used here is not a rigorous description of the fundamental reaction steps occurring during char gasification, however it is more convenient than the Langmuir–Hinselwood form and is a reasonable approximation when applied over a moderate range of pressure consistent with the original experiments. Table 1 provides the expressions for the intrinsic reactivity

of coal used in this work, while Fig. 5 shows data on the intrinsic reactivity of coal taken from the literature.

3.2 Mass balance

Chemical reaction at the wall involves a balance between the diffusion of reactants and products to and from the surface plus a consideration of the chemical kinetics of the reactions. Under pseudo-steady-state conditions a species mass balance at the wall surface yields:

$$\rho_w u_w Y_w^i + J_w^i = \dot{\omega}_w^i \qquad (i = 1, \ldots, N_g - 1), \tag{9}$$

where the mass diffusion flux normal to the wall is given by

$$J_w^i = -\rho_w \sum_{j=1}^{N_g} D_{eff,ij} \frac{\partial Y_w^i}{\partial n}. \tag{10}$$

In Eqs. (9)−(10), ρ_w, is the effective gas density at the wall, which is evaluated at the film conditions, ie. at the gas temperature and composition at the point mid−way
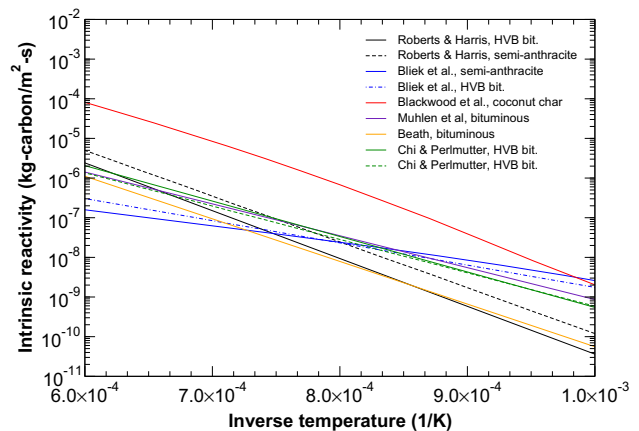
Fig. 5 Intrinsic reactivity of char to steam at 1MPa with a H_2O mole fraction of 0.2 for various coal chars reported in the literature extrapolated to typical coal gasification operating conditions (Data from Roberts 2000; Bliek et al. 1986; Blackwood and McGrory 1958; Muhlen et al. 1985; Beath 1996; Chi and Perlmutter 1989)

Table 1 Intrinsic reactivity expressions for coal gasification expressed in terms of molar concentrations

Reaction	Reactant gas	Pre-exponential factor, A_k (kg-char/m^2 s-[kmol/m^3]^n)	Pressure order , n	Activation energy , E_k (kJ/mol)	References
1	Oxygen	$2.503 \times 10^{+2}$	1.0	179.4	Smith (1978)
2	Carbon dioxide	8.593×10^{-1}	0.5	211.0	Roberts and Harris (2000)
3	Steam	$8.593 \times 10^{+0}$	0.5	231.0	Roberts and Harris (2000)
4	Hydrogen	2.337×10^{-6}	1.0	150.0	Tomita et al. (1977)

*$k_{f,k} = A_k T^n \exp(-E_k/RT)$

between the wall and the bulk gas. Substitution of Eq. (10) into Eq. (9) gives:

$$
-\rho_w u_w Y_w^i - \sum_{j=1}^{N_g-1} \rho_w D_{eff,ij} \frac{\partial Y_w^j}{\partial n} + \dot{\omega}_w^i = 0 \tag{11}
$$
$$
(i = 1, \ldots, N_g - 1).
$$

The N_g^{th} species mass fraction is determined as

$$
Y_w^{N_g} = 1 - \sum_{j=1}^{N_g-1} Y_w^j. \tag{12}
$$

The net mass flux normal to the surface is related to the net source of material formed from the chemical reactions by

$$
\rho_w u_w = \sum_{j=1}^{N_g} \dot{\omega}_w^j, \tag{13}
$$

and the species gradient term in Eq. (11) is discretised using

$$
\frac{\partial Y_w^i}{\partial n} \approx \frac{Y_w^i - Y_g^i}{\delta_{AB}}, \tag{14}
$$

where the length scale, δ_{AB}, is interpreted as an effective boundary layer thickness normal to the surface. It is calculated from the concentration boundary layer, δ_{AB}'', and the ash layer thickness according to:

$$
\delta_{AB} = \delta_{AB}'' + \frac{\tau}{\phi_{ash}} \delta_{ash}. \tag{15}
$$

Substitution of Eqs. (13) and (14) into Eq. (11) yields the final form required for defining the system of equations for the species mass balances:

$$
-\sum_{j=1}^{N_g} \dot{\omega}_w^j Y_w^i - \sum_{j=1}^{N_g-1} \rho_w \frac{D_{eff,ij}}{\delta_{AB}} \left(Y_w^i - Y_g^i \right) \\
+ \dot{\omega}_w^i = 0 \qquad (i = 1, \ldots, N_g - 1). \tag{16}
$$

The calculation of the term $D_{eff,ij}/\delta_{AB}$ depends on how the model will be used. When the model is used as a standalone program as discussed in this paper, the term can be interpreted as a mass transfer co-efficient and calculated from correlations in the literature. If the model is used as a submodel within a computational fluid dynamic model then the mass transfer through the boundary may be resolved and in this case, δ_{AB} takes the value of the distance from the surface to the centre of the adjacent control volume. The flux terms in Eq. (16) are given by

$$
\dot{\omega}_w^i = W_i \sum_{k=1}^{N_r} v_{i,k} r_k + \dot{\phi}_w^i, \tag{17}
$$

where the first term accounts for the contribution due to chemical reaction at the surface, and the second term

accounts for a sub-surface mass flux, the calculation of which is based on the proximate analysis of the coal as detailed in Sect. 3.5. In this model the chemical reaction rate, r_k, is based on the external surface of the wall and has units in kmol/m² s.

3.3 Multicomponent diffusion

Several methods can be used to describe the species diffusion in a multicomponent gas mixture. Fick's law of diffusion is a popular method, but is only applicable in a binary gas mixture or for highly diluted species in a carrier gas (Bird et al. 1960). Neither of these limiting cases is necessarily a good approximation for the gas mixture present during underground coal gasification. The general expression for the diffusion fluxes in multicomponent gas mixtures is given by the Stefan−Maxwell equations which are written as:-

$$
\nabla \cdot X_i = \sum_{j=1}^{n} \frac{1}{C_T D_{ij}} (X_i N_j - X_j N_i). \tag{18}
$$

After some manipulation these equations can be used to derive an effective diffusivity matrix, $[D_{eff}]$, for use in Eq. (10). In this case

$$
[D_{eff}] = [B]^{-1}, \tag{19}
$$

where $[B]$ is

$$
B_{ij} = (\delta_{ij} - 1) \left[\frac{X_g^i}{D_{iN}} \left(\frac{\bar{W}}{W_{N_g}} \right) - \frac{X_g^i}{D_{ij}} \left(\frac{\bar{W}}{W_j} \right) \right] \\
+ \delta_{ij} \left[-\sum_{n=1}^{N_g} \frac{X_g^n}{D_{in}} \left(\frac{\bar{W}}{W_i} \right) - \frac{X_g^i}{D_{iN_g}} \left(\frac{\bar{W}}{W_{N_g}} \right) \right]. \tag{20}
$$

The binary diffusivity between species i and j is calculated using the following formulae, taken from Bird et al. (1960):

$$
D_{ij} = 0.0188 \frac{\sqrt{T^3 \left(\frac{1}{W_i} + \frac{1}{W_j} \right)}}{P \sigma_{ij}^2 \Omega_{ij}}. \tag{21}
$$

3.4 Cavity growth rate

The cavity growth rate, v_c, is calculated based on the fraction of fixed carbon in the coal which is converted by reaction according to:

$$
v_c = \frac{\dot{\omega}_w^{fc}}{\rho_s Y_{pr}^{fc} X_c^{fc}}, \tag{22}
$$

where

$$
\dot{\omega}_w^{fc} = W_{fc} \sum_{k=1}^{N_r} r_{fc,k}, \tag{23}
$$

and a new parameter, X_c^{fc}—the coal fragmentation factor—is introduced to account for the thermomechanical behaviour of the coal. The fragmentation factor has values $0 < X_c^{fc} \leq 1$ and defines the degree of fixed carbon conversion due to chemical reaction that is obtained prior to thermomechanical failure of the solid matrix. From Eq. (22) values of X_c^{fc} less than unity cause an increase in the wall velocity. The value of X_c^{fc} is an input parameter in the model and must be either assumed or estimated from experiments.

3.5 Subsurface source terms

In order to have model closure it is necessary to define the subsurface mass flux terms, $\dot{\varphi}_w^i$, in Eq. (17). The calculation of the subsurface fluxes in the present model is based on the proximate analysis of the coal and an assumed thermo-mechanical spalling behaviour. The rates of formation of gaseous species are calculated using:

$$\dot{\varphi}_w^i = \dot{\varphi}_w^{vm,i} + \delta_{i,H_2O}\dot{\varphi}_w^{H_2O}, \tag{24}$$

where the first term represents fluxes of gas species resulting from pyrolysis of the volatile matter and the second term represents the gas flux of steam resulting from evaporation of liquid water. The volatile matter term is calculated from the rate of char reaction and the composition of the volatile matter with

$$\dot{\varphi}_w^{vm,i} = v_c\rho_s Y_{pr}^{vm,i}, \tag{25}$$

where the gas composition of the volatile matter, $Y_{pr}^{vm,i}$, are input parameters. The flux of steam is calculated using:

$$\dot{\varphi}_w^{H_2O} = v_c\rho_s Y_{pr}^w + \dot{\varphi}_l^{H_2O}, \tag{26}$$

where $\dot{\varphi}_l^{H_2O}$ represents a user defined liquid water influx rate. The water influx usually results from a driving force between the surrounding hydrostatic water pressure in the coal seam and the (lower) gas pressure, P_g, inside the cavity during UCG operations. It may be estimated using a simple Darcy equation or determined by separate hydrogeological modelling.

In the model, if $X_c^{fc} < 1$ then the unconverted char is also released from the wall. The calculation of the solid material which detaches from the wall is performed with the following equations:

$$\dot{\omega}_f^{fc} = v_c\rho_s Y_{pr}^{fc}(1 - X_c^{fc}), \tag{27}$$

and

$$\dot{\omega}_f^{ash} = v_c\rho_s Y_{pr}^{ash}. \tag{28}$$

From Eq. (28) it can be seen that under the pseudo-steady-state assumption the ash is assumed to segregate from the

wall as it is formed, even though a fixed thickness of the ash layer, δ_{ash}, may be prescribed by the user. Equations (24)−(28) enable all terms in the surface mass balance, Eq. (16), to be calculated.

3.6 Energy balance

Derivation of the energy balance also assumes a pseudo-steady-state and hence a balance between energy transferred to the surface due to radiation and convection and energy consumed by chemical reactions and conducted into the coal. The conservation of energy at the wall is given by:

$$-\varepsilon\sigma\left(T_w^4 - T_g^4\right) - \lambda_g\frac{\partial T_w}{\partial n} - \sum_{k=1}^{N_r} r_k\Delta H_{r,k} - q_w = 0, \tag{29}$$

where the first term on the left represents the radiant heat transfer to the surface from the surroundings, the second term represents the heat transfer due to conduction, the third term represents the total heat release at the surface due to chemical reactions at the surface and the fourth term represents a heat flux into the surface to account for heating of reactants to the surface temperature and other subsurface heat losses. A view factor of unity is assumed in the model. Discretisation of Eq. (29) gives

$$-\varepsilon\sigma\left(T_w^4 - T_g^4\right) - \frac{\lambda_g}{\delta_T}\left(T_w - T_g\right) - \sum_{k=1}^{N_r} r_k\Delta H_{r,k} - q_w = 0, \tag{30}$$

where δ_T is a length scale interpreted as the effective thermal boundary layer thickness when the model is used as a standalone application. The mass and energy balance equations need to be solved together in order to determine the surface compositions Y_w^i $(i = 1, ..., N_g - 1)$ and the wall temperature T_w, which can be used to determine the rate of the surface chemical reactions and the cavity growth rate, v_c.

3.7 Subsurface heat flux

The net heat flux into the material can be determined using:

$$\begin{aligned}
q_w = v_c\rho_s\big[&C_{p,s}\left(T_{dry} - T_{amb}\right) \\
&+ C_{p,s}\left(1 - Y_{pr}^w\right)\left(T_{vm} - T_{dry}\right) \\
&+ C_{p,s}\left(1 - Y_{pr}^w - Y_{pr}^{vm}\right)\left(T_w - T_{vm}\right) \\
&+ C_{p,g}Y_{pr}^w\left(T_w - T_{dry}\right) \\
&+ C_{p,g}Y_{pr}^{vm}(T_w - T_{vm}) + Y_{pr}^w\Delta H_{vap}\big] \\
&+ \dot{\varphi}_l^{H_2O}\Delta H_{vap}
\end{aligned} \tag{31}$$

where the first three terms account for the sensible heating of the solid, the fourth and fifth terms account for sensible

heating of the gas, the sixth term accounts for the evaporation of moisture bound in the coal, and the last term accounts for the evaporation of water which reaches the wall as a flux due to migration through the solid. For simplicity, it is assumed that the volatile matter is released at the temperature:

$$T_{vm} = T_{dry} + \frac{1}{2}\left(T_w - T_{dry}\right). \tag{32}$$

The heat capacities are taken to be constant with values of $C_{p,g} = 1900$ J/kg K and $C_{p,s} = 1458$ J/kg K. The drying front temperature, T_{dry}, is calculated from the vapour pressure relationship given by Thorsness et al. Thorsness et al. (1978):

$$T_{dry} = \frac{4690.0}{12.61 - \ln(P_g/101325.0)}, \tag{33}$$

and the latent heat of vaporisation of water, ΔH_{vap}, is calculated using a 4th order polynomial in temperature fitted to the tabulated data given by van Wylen and Sonntag (1985).

3.8 Boundary conditions

The boundary conditions for the solution of Eqs. (16) and (30) are the values for the bulk gas compositions Y_g^i $(i = 1, ..., N_g - 1)$, the bulk gas temperature T_g and bulk gas pressure, P_g. When the model is used as a standalone application, these boundary conditions are prescribed by the user, while when the model is incorporated into a reactor model, such as CFD, these boundary conditions are calculated at each iteration of the main solver. In the coal, the ambient temperature, T_{amb}, and the liquid water influx, $\dot{\varphi}_l^{H_2O}$, are user defined boundary conditions. The properties of the coal, namely the density, ρ_s, proximate analysis $(Y_{pr}^{fc}, Y_{pr}^{vm}, Y_{pr}^{ash}, Y_{pr}^w)$, the composition of the volatile matter, $Y_{pr}^{vm,i}$, and the coal fragmentation factor, X_c^{fc}, must also be defined.

4 Numerical methods

When the model is used as a standalone application, an iterative procedure is used to solve for the coupled mass and energy balances at the wall. An outer iterative loop is used to solve for the combined problem, with sequential inner loops to solve for the mass balance equations and the energy balance equation. Figure 6 shows an overview of the numerical procedure that is applied by the model. The model is coded in C.

The solution starts by setting the boundary conditions, namely the bulk gas compositions, temperature and
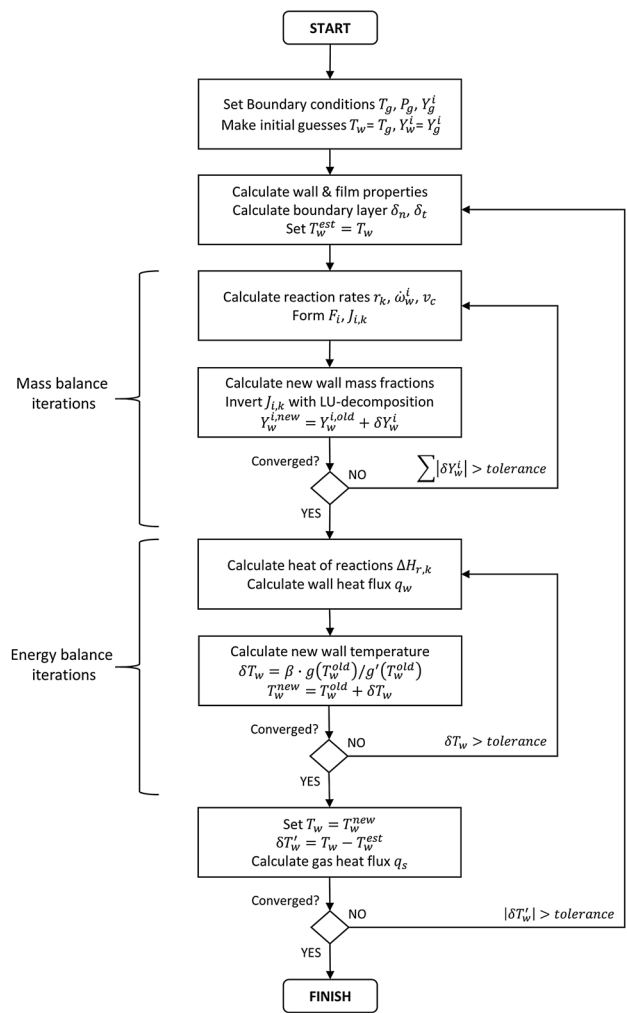

Fig. 6 Overview of the numerical procedure used to calculate the cavity growth rate at a coal wall

pressure. In the standalone model these are specified by the user for each problem. Initial guesses for the gas compositions and temperature at the wall are also made and the estimated wall temperature is stored, $T_w^{est} = T_w$. Newton's method is used to solve for the mass balance, whereby the following function is formed from Eq. (16):

$$F_i = -\sum_j \dot{\omega}_w^j Y_w^i - \rho_g h_{m,i}(Y_w^i - Y_g^i) + \dot{\omega}_w^i, \tag{34}$$

and is expanded in a Taylor series in the neighbourhood of the current solution $\mathbf{Y}_w$. In matrix notation this expansion yields:

$$\mathbf{F}(\mathbf{Y}_w + \delta\mathbf{Y}_w) = \mathbf{F}(\mathbf{Y}_w) + \mathbf{J} \cdot \delta\mathbf{Y}_w + O(\delta\mathbf{Y}_w^2). \tag{35}$$

By setting $\mathbf{F}(\mathbf{Y}_w + \delta\mathbf{Y}_w) = 0$ in Eq. (35) and neglecting the higher order terms a linear system of equations is obtained for the surface mass fraction corrections $\delta\mathbf{Y}_w$ that move the set of mass balance equations, such that $|\mathbf{F}| \rightarrow 0$,

$$F_i = -J_{i,k}\, \delta Y_w^i. \tag{36}$$

The linear system is solved at each iteration for the mass fraction corrections $\delta \mathbf{Y}_w$ using the *LU*-decomposition method (Press et al. 1992). The new surface mass fractions are then updated, $Y_w^{i,new} = Y_w^{i,old} + \delta Y_w^i$, and the procedure repeated until a specified error tolerance is met. The entries in the Jacobian matrix $J_{i,k}$ are given by $J_{i,k} = \frac{\partial F_i}{\partial Y_w^k}$ which can be expanded to:

$$J_{i,k} = -\sum_j \left(\frac{\partial \dot{\omega}_w^j}{\partial Y_w^k} Y_w^i + \delta_{i,k} \dot{\omega}_w^j \right) - \delta_{i,k} \rho_w \frac{D_{eff,ik}}{\delta_{AB}} + \frac{\partial \dot{\omega}_w^i}{\partial Y_w^k}, \tag{37}$$

where the derivative of the $\dot{\omega}_w^i$ term with respect to each of the component mass fractions, Y_w^i, is determined from $\frac{\partial \dot{\omega}_w^i}{\partial Y_w^k} = W_i \sum_r \frac{\partial r_r}{\partial Y_w^k}$, which is computed using Eq. 6 and utilizing the chain rule by noting that $C_j = \frac{\rho_g Y_w^j}{W_j}$.

To solve for the energy balance Eq. (30), a variant of Newton's method known as fixed point iteration is used to find the wall temperature, T_w. The new wall temperature is calculated with:

$$T_w^{new} = T_w^{old} - \beta \frac{g(T_w^{old})}{g'(T_w^{old})}, \tag{38}$$

where

$$g(T_w) = \varepsilon \sigma \left(T_w^4 - T_g^4 \right) + \frac{\lambda_g}{\delta_T} \left(T_w - T_g \right) + \sum_{k=1}^{N_r} r_k \Delta H_{r,k} + q_w, \tag{39}$$

and

$$g'(T_w) = 4\varepsilon\sigma\left(T_w^3\right) + \frac{\lambda_g}{\delta_T}, \tag{40}$$

and β is an under-relaxation factor which is normally set at 0.01 to give good numerical stability. The energy balance iterations are continued until the change in wall temperature, $\delta T_w = T_w^{new} - T_w^{old}$, is reduced below a specified convergence tolerance. A check is also performed to ensure that the heat flux from the bulk gas to the wall is equal to the heat flux into the material according to Eq. (31).

The outer loop iterations over the combined mass and energy balance problem are continued until the new wall temperature, T_w^{new}, calculated by the energy balance is within a specified tolerance of the estimated wall temperature, T_w^{est} calculated at the start of the loop. When the conservation of mass and energy equations are in balance then the submodel finishes with a solution for the component mass fractions at the wall, Y_w^i, the wall temperature, T_w, the reaction rates, r_k, the species fluxes $\dot{\omega}_w^i$, subsurface source terms, $\dot{\phi}_w^i$, the cavity growth rate, v_c and other derived quantities.

When the model is used within a reactor model, the solution of the energy balance equations are handled by the reactor model and only the inner mass balance iterations are used to find the solution at the wall, namely reaction rates and species mass fractions. An example of coupling an earlier version of the model with CFD has been presented by Perkins and Sahajwalla (2007).

5 Model validation

In this section calculations from the model are compared to laboratory combustion experiments on coal cores and coal blocks and also to calculated values of cavity growth rates from several UCG field trials. For each simulation 10 gas species were assumed: O_2, CO, CO_2, H_2, H_2O, CH_4, C_2H_6, H_2S, TAR and N_2, where TAR is used to represent condensable hydrocarbons at room temperature and was assumed to be benzene for simplicity. The composition of the volatile matter of each coal, $Y_{pr}^{vm,i}$, was determined from a mass balance based on the proximate and ultimate analysis of the coal. The composition of the volatile matter for the Chinchilla coal used in most of the simulation runs was found to be: $Y_{pr}^{vm,CO} = 0.135$, $Y_{pr}^{vm,CO_2} = 0.370$, $Y_{pr}^{vm,H_2} = 0.045$, $Y_{pr}^{vm,H_2O} = 0.0223$, $Y_{pr}^{vm,CH_4} = 0.170$, $Y_{pr}^{vm,C_2H_6} = 0.0605$, $Y_{pr}^{vm,H_2S} = 0.0082$, $Y_{pr}^{vm,TAR} = 0.170$, $Y_{pr}^{vm,N_2} = 0.019$.

5.1 Comparison with coal core experiments

In this section the submodel is used to simulate laboratory combustion experiments on Texas lignites conducted by Poon at the University of Texas at Austin (1985). In the combustion experiments, Poon measured the burning rates of Texas lignite cores by using gas injection located near the surface of the coal sample and being directed across the surface. The experiments were conducted at atmospheric pressure using varying levels of oxygen enrichment in the feed gas stream.

The effective boundary layer thickness used to represent the experimental conditions is calculated from a correlation for forced convection mass transfer Wylen and Sonntag (1985), using:

$$\text{Sh} = \frac{h_m L}{D_{im}} = 0.664 \text{Re}^{0.5} \text{Sc}^{0.33}, \tag{41}$$

where the characteristic length, L, is set equal to the diameter of the coal cores, which was $L = 2.54$ cm. Since $h_m = D_{im}/\delta_{AB}''$, then δ_{AB}'' can be calculated as $\delta_{AB}'' = L/\text{Sh}$

using the Sherwood correlation above. The boundary conditions for this problem are given by the gas composition and a bulk gas temperature of $T_g = 400$ K. The coal density is taken to be $\rho_s = 1230$ kg/m^3 and the pressure is atmospheric pressure.

Table 2 provides the proximate analysis of the dry and wet Texas lignite used in the experiments. In Fig. 7, model simulations are compared to experimental measurements of the burn rate as a function of oxygen concentration (mole fraction) in the blast gas for the dry coal and the wet coal. The model simulations agree very well with the experiments. It is observed that the model accurately predicts the dependence on oxygen concentration and also predicts a higher burn rate for the wet coal, due to the enhancement of the steam-char reaction. In Fig. 8, model simulations are compared to experimental measurements of the burn rate as a function of blast gas velocity for two oxygen concentrations. Again the model simulations agree very well with the experimental measurements. It should be noted in that in these combustion experiments the mass transfer of oxygen from the bulk gas to the coal surface is the rate

controlling step, so these experiments do not really test the modelling of the intrinsic chemical reactivity of the char.

5.2 Comparison with coal block experiments

Prabu and Jayanti (2012) have conducted combustion experiments using small blocks of thermal coal, with typical dimensions of $\sim$ 0.1–0.25 m width, $\sim$ 0.09–0.12 m height and $\sim$ 0.2–0.28 m length. The experiments were conducted at atmospheric pressure using pure oxygen over a period of 10 h. Three flow rates of oxygen at 1 lpm (0.06 Nm^3/h), 1.25 lpm (0.076 Nm^3/h) and 1.5 lpm (0.09 Nm^3/h) were injected into the coal blocks for a period of 10 h through a small channel of 0.01 m width after ignition had been achieved. Throughout the experiments, temperatures in the block and the product gas composition were measured. At the end of the experiments, the shape and volume of the cavity formed was recorded. Table 3 provides a summary of the oxygen flow rate and calculated growth rates based on the experimental observations for three runs using Coal-2 (Prabu and Jayanti 2012).

The coal density is reported as $\rho_s = 1225$ kg/m^3, the pressure is atmospheric pressure, $P_g = 101,325$ Pa and the bulk gas temperature, T_g, is set to 650 ^{o}C based on the experimental measurements. The proximate analysis of the coal was: fixed carbon 41.6 wt%, volatile matter 28.8 wt%, ash 19.2 wt% and moisture 10.4 wt%. The flow is laminar and a mass transfer correlation for flow in a pipe is used to represent the mass transfer process from the bulk gas to the wall:
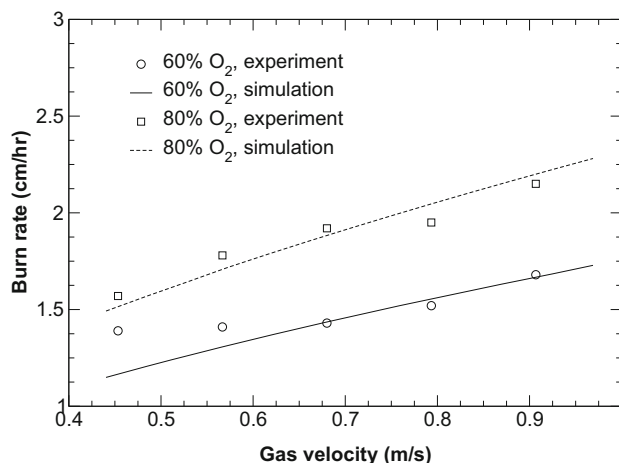
$$\text{Sh} = \frac{h_m L}{D_{im}} = 1.82 \text{Re}^{0.33} \text{Sc}^{0.33}, \tag{42}$$

Table 2 Proximate analysis of Texas lignite used in the experimental work of Poon (1985)

Proximate analysis	Weight (%)	
	Dry coal	Wet coal
Moisture	7.5	33.0
Volatile matter	50.5	35.0
Fixed carbon	30.5	24.5
Ash	11.5	7.5
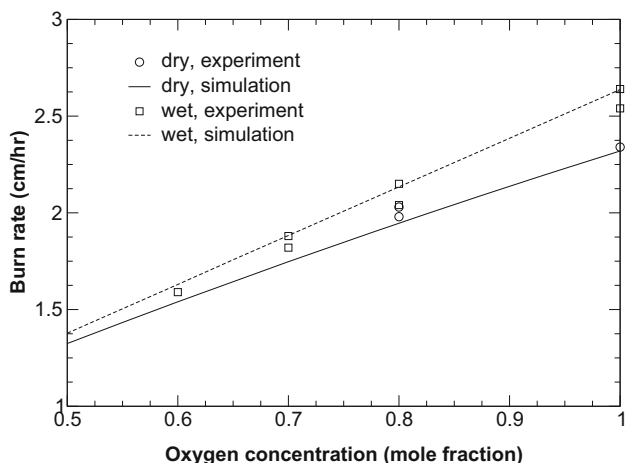
Fig. 7 Effect of oxygen concentration and coal moisture on the combustion rate of lignite cores

Fig. 8 Effect of gas velocity and oxygen concentration on the combustion rate of lignite cores

Table 3 Results for three runs of laboratory coal block combustion and gasification (data derived from Prabu and Jayanti 2012)

Run No.	Flow rate (m^3/h)	Bottom growth (cm)	Top growth (cm)	Average growth (cm)	Hours (h)	Growth rate (cm/h)	Growth rate (m/day)
2	0.060	3.5	1.7	2.6	10	0.26	0.0624
3	0.075	2.0	3.6	2.8	10	0.28	0.0672
4	0.090	3.7	2.9	3.3	10	0.33	0.0792

where the characteristic length L, is set equal to the diameter of the initial channel placed in the coal block, of $L = 0.01$ m. In the simulations the ash layer has been set at $\delta_{ash} = 2.5$ cm, to capture the fact that ash builds up as the coal char is reacted away and impedes the diffusion of oxygen to the surface of the coal. Model simulations are compared to the calculated growth rates from the experiments as a function of oxygen flow rate in Fig. 9. While the model forecasts higher cavity growth at higher oxygen flow, the effect is underpredicted in comparison to the experiments. At the highest oxygen flow of 0.09 Nm^3/h the growth rate is underpredicted by about 17 %. It should be noted that the model predictions of cavity growth rate are sensitive to the ash layer and its impact on the mass transfer of oxygen from the bulk gas to the wall. In fact, it was found that multiple combinations of values for the bulk gas temperature and ash layer thickness can give similar cavity growth rate results. For example, at an oxygen flow of 0.075 Nm^3/h a growth rate of $v_c = 0.0672$ m/day can be obtained with each of the following conditions, which are all reasonable based on the reported experimental measurements: $T_g = 700\ ^oC$ and $\delta_{ash} = 2.74$ cm ; $T_g = 650\ ^oC$ and $\delta_{ash} = 2.47$ cm ; $T_g = 600\ ^oC$ and $\delta_{ash} = 2.27$ cm.

5.3 Comparison with field trials

Comparing model predictions with field trial data is complicated by a range of factors. Since the cavity shape is generally inferred from a small number of core and/or thermocouple wells and mass and energy balance calculations, the calculated cavity growth rates can only be considered as rough estimates. In this work, the cavity growth rate is calculated using reported data from each trial based on the point farthest from the line connecting the injection and production wells. In addition, measurements of the char structure and reactivity under in situ conditions have not been reported in the literature for many of the coals used in previous field trials, so in this work reactivity data from sub-bituminous coals obtained under laboratory conditions has been used (Roberts and Harris 2000). The ash layer thickness has been assumed to be $\delta_{ash} = 5$ cm and the thermo-mechanical properties of the coals have been
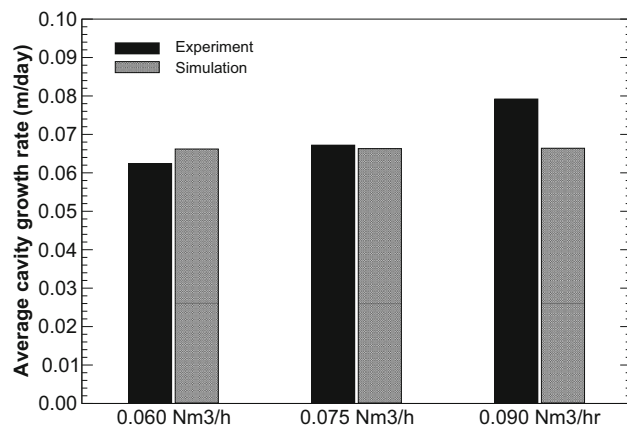
Fig. 9 Effect of oxygen flow rate on the cavity growth rate in laboratory coal block combustion experiments

set at $X_c^{fc} = 0.8$ since no direct measurements or reliable correlations exist regarding the thermo-mechanical behaviour of coal as a function of site conditions, operating conditions and parent coal properties. Field trials of UCG are usually operated using an oxidant of air or a steam/oxygen mixture. In this work, the bulk gas temperature has been set at $T_g = 1400$ K for air blown trials and $T_g = 1500$ K for oxygen blown trials based on earlier simulation work (Perkins and Sahajwalla 2008). Similarly, a standard bulk gas composition has been assumed for air blown and steam/oxygen blown operation as shown in Table 4. The UCG trials considered include the Hanna I, Pricetown, Large Block Experiment No. 5 (LBK-5), Partial Seam CRIP (PSC), Rocky Mountain I CRIP (RM I) cavity number 2 and Chinchilla Gasifier 5 (G5) cavity number 1 - for both lateral and vertical cavity growth. Most of these trials were only operated for a few weeks and hence the cavity growth estimated from field trial data is actually representative of early cavity growth, where the combustion zone is in close proximity to the lateral extent of the evolving cavity. The exception is for the lateral cavity growth of G5 cavity 1 which operated for 183 days. In this case, a lower bulk gas temperature of $T_g = 1000$ K has been used to represent the fact that the combustion zone is further from the lateral extent of the cavity. The vertical cavity growth rate for G5 cavity 1 is estimated using

Injected gas	Air	Steam/oxygen
CO	0.08	0.13
CO_2	0.12	0.20
H_2	0.16	0.27
H_2O	0.20	0.33
CH_4	0.04	0.07
N_2	0.40	0.00
H_2O/dry gas ratio	0.25	0.50

thermocouple data from the first 5 days of operation and hence the bulk gas temperature of $T_g = 1400$ K is used for this case. Based on reported mass balances the water influx is estimated to be on the order of $\dot{\phi}_l^{H_2O} \sim 0.001$ kg/m^2 s for most of the trials. Table 5 provides basic operating data for each of the UCG field trials.

To capture the heat and mass transfer effects, the thermal and concentration boundary layers are estimated using correlations. In underground coal gasification, natural convection dominates over forced convection in the void spaces (Perkins 2018b). An appropriate correlation for the Sherwood number (Sh) is given by Kuyper (1994):

$$Sh = 0.0595 Gr^{0.33} Sc^{0.33}, \tag{43}$$

where the Grashof number (Gr) is defined as:

$$Gr = 9.81 \frac{\rho_g (\rho_g - \rho_w) H^3}{\mu_g^2}, \tag{44}$$

and ρ_g is the bulk gas density adjacent to the wall. In this situation the boundary layer thickness is calculated as:-

$$\delta_{AB}'' = \frac{H}{Sh}. \tag{45}$$

Interestingly, using the above correlation results in the boundary layer thickness being independent of the length scale H. The thermal boundary layer thickness is calculated analogously:

$$\delta_T = \frac{H}{Nu}, \tag{46}$$

where

$$Nu = 0.0595 Gr^{0.33} Pr^{0.33}. \tag{47}$$

Figure 10 compares the estimated cavity growth rates with model simulations. Cavity growth in sub-bituminous coals tends to be between 0.5 and 1 m/day during early cavity growth, and the model tends to over-predict the average growth rate by $\sim 20\%$. The average lateral growth rate

over 183 days of air blown gasification in the Chinchilla G5 trials is quite low at 0.03 m/day based on thermocouple data (Mashego 2013). While the simulation model does predict a lower growth rate for this case, it is substantially higher at ~ 0.08 m/day. The initial vertical cavity growth rate in the Chinchilla trial was calculated to be 0.47 m/day compared with a simulation forecast of 0.59 m/day.

Differences between the observed and simulated rates are most likely due to uncertainties in temperature, water influx and/or thermo-mechanical behaviour of the coal which can all have a large impact on the calculated rates (Perkins and Sahajwalla 2006). Overall the model simulations provide estimates of cavity growth rates which are comparable in magnitude to those observed. Improved predictions really require the incorporation of the cavity growth submodel within a reactor model so that simulations can also be matched to the overall mass and energy balance of the UCG trial.

6 Simulation results of the combustion zone

During the early stages of underground coal gasification, oxygen injected with the oxidant may reach and directly react with the exposed coal surface. As coal is consumed and the environment around the injection point heats up, it is expected that most of the oxygen will be consumed in the gas phase via reactions with volatiles released by the coal. In this section, the model is used to forecast cavity growth rates when oxygen is present in the bulk gas close to the surface of coal char, in the so-called combustion zone. The oxidants considered include air, oxygen enriched air and steam/oxygen mixtures, with a molar ratio, r, of steam to oxygen in the range of 1:1 to 4:1. Most previous UCG field trials using steam/oxygen have been undertaken with a ratio of $2 \leq r \leq 3$ (Perkins and Vairakannu 2017). Table 6 shows the composition of the injected oxidants.

The simulation study is undertaken with the sub-bituminous coal properties of the Chinchilla G5 UCG project shown in Table 5, and assumes the following operating conditions: $T_g = 1400$ K, $P_g = 750$ kPa, $\dot{\phi}_l^{H_2O} = 0.0$ kg/m^2 s, $X_c^{fc} = 1.0$. The ash layer is selected as $\delta_{ash} = 0$ m and $\delta_{ash} = 0.02$ m to highlight the impact of ash buildup. The boundary layer thickness is assumed to be fixed at $\delta_{AB} = \delta_T = 2.0 \times 10^{-3}$ m which represents a strong forced / natural convective flow (Perkins 2018b).

6.1 Effect of the ash layer

An ash layer is expected to build up on the surface of the coal char as combustion and gasification reactions proceed. Lin et al. (2016) studied the reactions occurring in the ash

Table 5 Basic operating data for UCG field trials

	Hanna I	Pricetown	LBK-5	PSC	RM 1	Chinchilla G5 lateral	Chinchilla G5 vertical
Year of field trial	1973	1979	1983	1983	1987	2013	2013
Coal properties							
Type	Sub-bit.	Hvc bit.	Sub-bit	Sub-bit.	Sub-bit.	Sub-bit.	Sub-bit.
Density (kg/m³)	1363	1360	1384	1390	1390	1400	1400
Seam thickness (m)	11	1.8	10.2	5.0	9.1	5.5	5.5
Proximate analysis							
Fixed carbon (wt%)	35.5	49.5	35.5	28.0	30.8	26.7	26.7
Volatile matter (wt%)	28.5	38.1	28.5	34.0	31.7	31.4	31.4
Ash (wt%)	14.4	11.0	14.4	21.0	28.9	32.7	32.7
Moisture (wt%)	21.6	1.4	21.6	17.0	8.6	9.3	9.3
Operating conditions							
Injected gas	Air	Air	$H_2O : O_2$	$H_2O : O_2$	$H_2O : O_2$	Air	Air
Temperature (K)	1400	1400	1500	1500	1500	1000	1400
Pressure (kPa)	150	2100	150	430	500	750	750
Water influx (kg/m² s)	1.65e-6	1.34e-3	1.79e-3	1.27e-3	9.60e-4	5.67e-4	7.23e-4
References	Cena and Thorsness (1981)	Cena and Thorsness (1981); Eddy and Schwartz (1983)	Hill and Thorsnes (1982); Thorsness and Cena (1983)	Cena et al. (1987); Britten and Thorsness (1989); Hill et al. (1984)	Boysen et al. (1998)	Perkins et al. (2016); Mashego (2012, 2013)	Perkins et al. (2016); Mashego (2012, 2013)
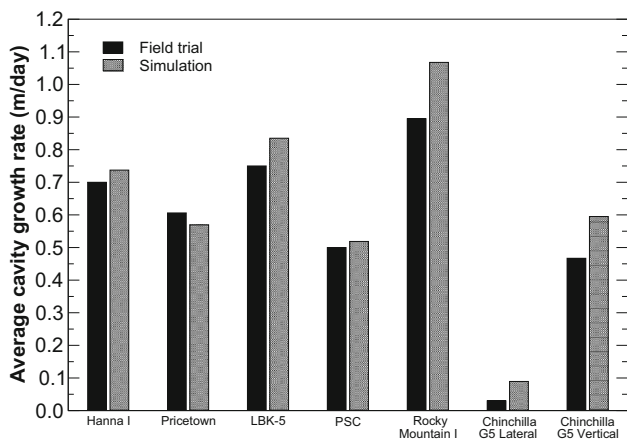
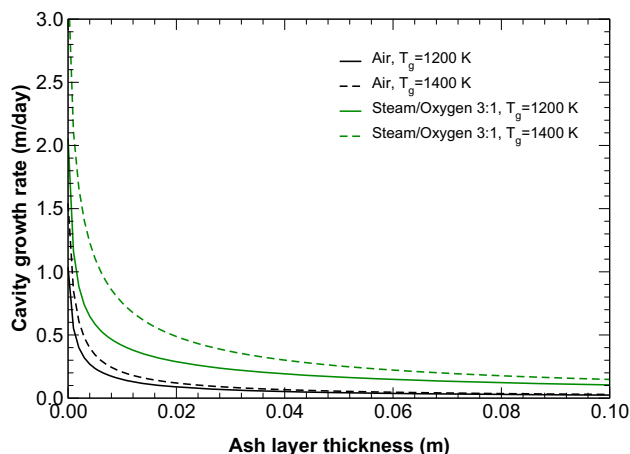**Fig. 10** Comparison of estimated cavity growth rates for the UCG field trials with results from the cavity growth submodel

Fig. 11 Effect of ash layer thickness on the cavity growth rate for two oxidants and two gas temperatures in the combustion zone

Table 6 Bulk gas compositions (mole fraction) used to represent the combustion zone of underground coal gasification

Injected gas	Air	Enriched air	Steam/oxygen
O_2	0.21	0.50	$\frac{1}{1+r}$
H_2O	0.00	0.00	$1 - \frac{1}{1+r}$
N_2	0.79	0.50	0.00
Steam/oxygen ratio	n/a	n/a	r

layer of a low volatile bituminous coal. When small cylindrical cores were exposed to combustion conditions at 1250 °C for 40 h, the ash layer thickness was measured to be about 7 mm. Lin et al. also observed that once the ash layer was greater than 1.3 mm in thickness, CO started to be combusted in the ash layer raising the temperature above the char surface temperature (Lin et al. 2016). In the current 0-dimensional model, all reactions are assumed to occur at the char surface, so the combustion reaction, Eq. (2), is used to represent the overall conversion of char to CO_2, as the two step process, whereby CO is combusted in the gas phase, cannot be resolved by the model.

In coal block gasification experiments, Prabu and Jayanti observed zones of ash that were several centimetres thick (Prabu and Jayanti 2012, 2014). While, laboratory experiments show ash layer build up, it is not easy to obtain good estimates of the psuedo-steady average ash layer thickness from field trials. It should also be recognized that the ash will likely build up towards the bottom of the cavity, impeding heat and mass transfer in the lower regions, while coal char may remain exposed in the upper regions of the coal seam. Thus, the effective ash layer thickness is likely to vary by location on the coal surfaces. Based on observations from laboratory experiments and

excavations of field trials the average ash layer thickness is expected to be between a few millimetres and a few centimetres.

The effect of the ash layer on cavity growth rate is shown in Fig. 11. Even small increases in the thickness of the ash layer have a material impact on the mass transfer of oxygen and syngas products to and from the surface of the char. In Fig. 11, results for air and an oxidant with a steam/oxygen in a molar ratio of 3:1 are shown. When an ash layer is present, it has been found that the ratio of steam to oxygen in the oxidant has only a small effect on the cavity growth rate.

6.2 Effect of temperature

While the combustion reaction of oxygen with char is exothermic, the bulk gas temperature still influences the observed cavity growth rates. Figure 12a shows the impact of the choice of oxidant and gas temperature on cavity growth rate when there is no ash layer, $\delta_{ash} = 0$ m. It can be seen that at a given temperature the cavity growth rate is correlated to the oxygen content in the oxidant. At low temperatures the cavity growth rate is proportional to the oxygen concentration, however at high temperature the presence of steam in the oxidant can also contribute significantly to the overall cavity growth rate. The impact of steam in the oxidant is most easily understood by comparing the results for enriched air ($N_2/O_2=1:1$) with steam/oxygen ($H_2O/O_2=1:1$). Figure 12b shows equivalent results when the ash layer is present with a thickness of $\delta_{ash} = 0.02$ m. It can be seen that the presence of the ash layer substantially reduces the cavity growth rate due to the reduction in mass transfer of reactants from the bulk gas to the char surface.
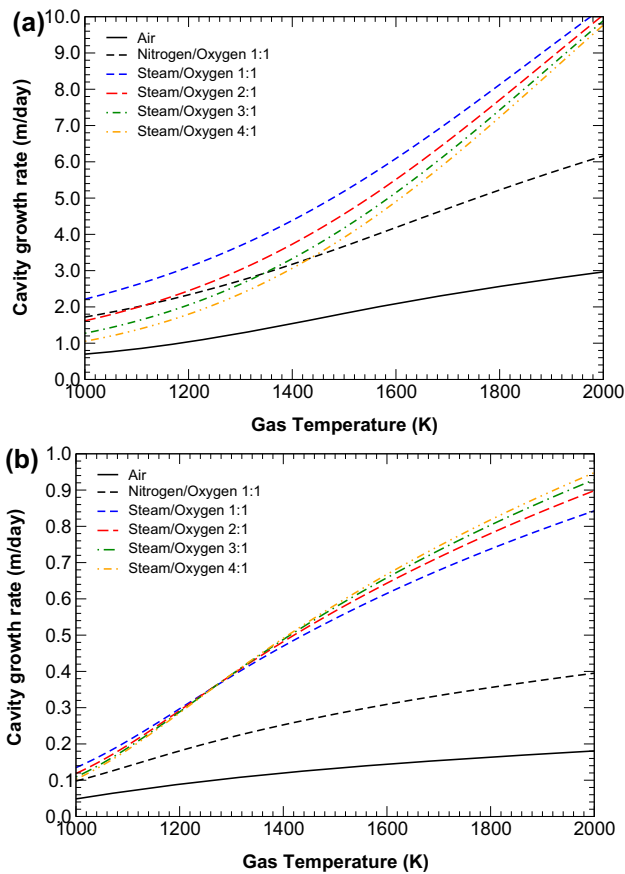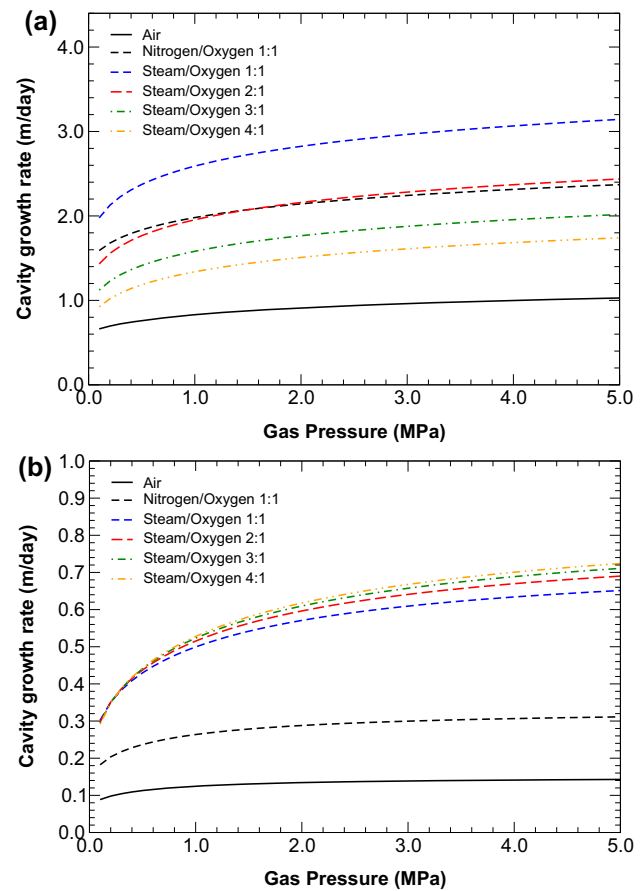
Fig. 12 Effect gas temperature and oxidant on cavity growth rate in the combustion zone for: **a** $\delta_{ash} = 0$ m and **b** $\delta_{ash} = 0.02$ m

Fig. 13 Effect of gas pressure and oxidant on the cavity growth rate in the combustion zone for: **a** $\delta_{ash} = 0$ m and **b** $\delta_{ash} = 0.02$ m
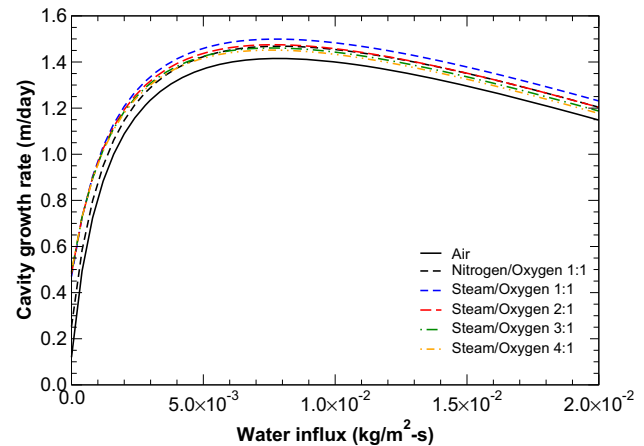
6.3 Effect of pressure

Figure 13 shows how the gas pressure and oxidant choice effect the cavity growth rate. Higher pressure increases the cavity growth rates due to the positive impact on mass transfer. Figure 13a shows the results when there is no ash layer present and it can be seen that cavity growth at low pressure is in the range $0.6 \lesssim v_c \lesssim 2.0$ m/day, whereas at high pressure the range can be $1.0 \lesssim v_c \lesssim 3.0$ m/day. When an ash layer is present the cavity growth rates reduce to $0.1 \lesssim v_c \lesssim 0.8$ m/day depending upon the oxidant selected, as seen in Fig. 13b.

6.4 Effect of water influx

The effect of the water influx rate and oxidant on the cavity growth rate for an ash layer thickness of $\delta_{ash} = 0.02$ m is shown in Fig. 14. It can be seen that the cavity growth is correlated to the concentration of oxygen in the bulk gas, with the highest rates observed with a steam/oxygen ratio of $r = 1{:}1$, and the lowest rates observed when air is used as the oxidant. In general, greater water influx increases the cavity growth rate for values of the water influx less than

Fig. 14 Effect of water influx and oxidant on the cavity growth rate in the combustion zone for an ash layer thickness of $\delta_{ash} = 0.02$ m

$\sim 7 \times 10^{-3}$ kg/m^2 s, and reduces the cavity growth rate at higher water influx rates. This is explained by the ash layer which impedes the rate at which steam can reach the char surface from the bulk gas. Addition of water influx increases the concentration of steam at the char surface,

enhancing the steam gasification reaction. However, at high water influx rates, the energy penalty associated with evaporating excess water reduces the char surface temperature and therefore the cavity growth rate. Figure 14 shows that the observed cavity growth rate is quite sensitive to water influx. However, it should be noted that the current simulations assume a fixed gas temperature of $T_g = 1400$ K − in practice increasing the water influx will increase heat transfer from the gas to the wall, lowering the gas temperature, and thereby reducing the sensitivity of the observed growth rate.

7 Simulation results of the gasification zone

In the gasification zone, there is no oxygen in the vicinity of the coal wall, since the the oxygen injected into the formation has been consumed in the combustion zone. However, the gas temperature is still very high due to the heat release from the combustion zone and participates in radiant heat exchange with the exposed coal surfaces. In this section, the model is used to investigate the impact of different operating conditions on the cavity growth rate in the gasification zone. The coal properties and operating conditions are assumed to be the same as in Sect. 6 unless otherwise indicated. The bulk gas compositions assumed in the gasification zone for air blown and steam/oxygen blown gasification are given in Table 4.

7.1 Effect of the ash layer

The effect of the ash layer, oxidant and gas temperature on cavity growth rate in the gasification zone is shown in Fig. 15. As in the combustion zone, small increases in the thickness of the ash layer have a material impact on the cavity growth rate calculated by the model.

7.2 Effect of temperature

In the gasification zone, the gas temperature is the primary driver for sustaining the gasification reactions at the surface of the coal wall. Figure 16 shows the impact that the gas temperature and oxidant has on the cavity growth rate for no water influx and a water influx of 2×10^{-3} kg/m^2 s with an ash layer thickness of $\delta_{ash} = 0.02$ m. It can be seen that without water influx the cavity growth rates are in the range $0.1 \lesssim v_c \lesssim 0.5$ m/day. When additional water is added, the cavity growth rate increases significantly indicating that the concentration of steam at the surface is deficient for the char−steam reaction. However, as discussed in Sect. 6.4, in a real UCG system, the additional water influx would reduce the gas temperature and the overall impact on cavity
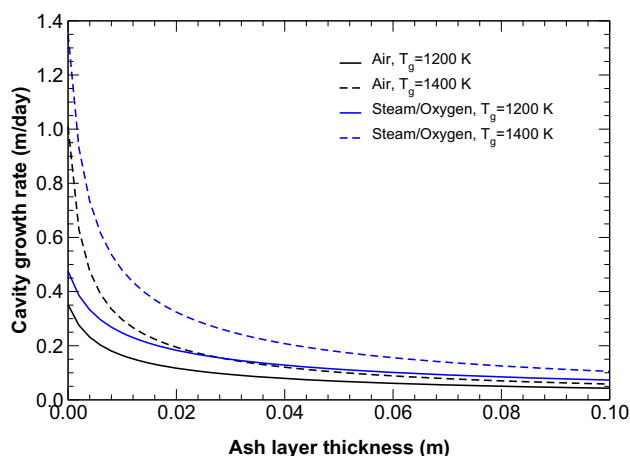

Fig. 15 Effect of ash layer thickness on the cavity growth rate for two oxidants and two gas temperatures in the gasification zone
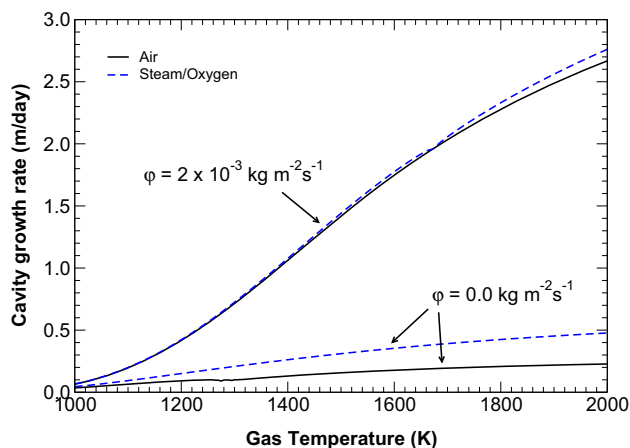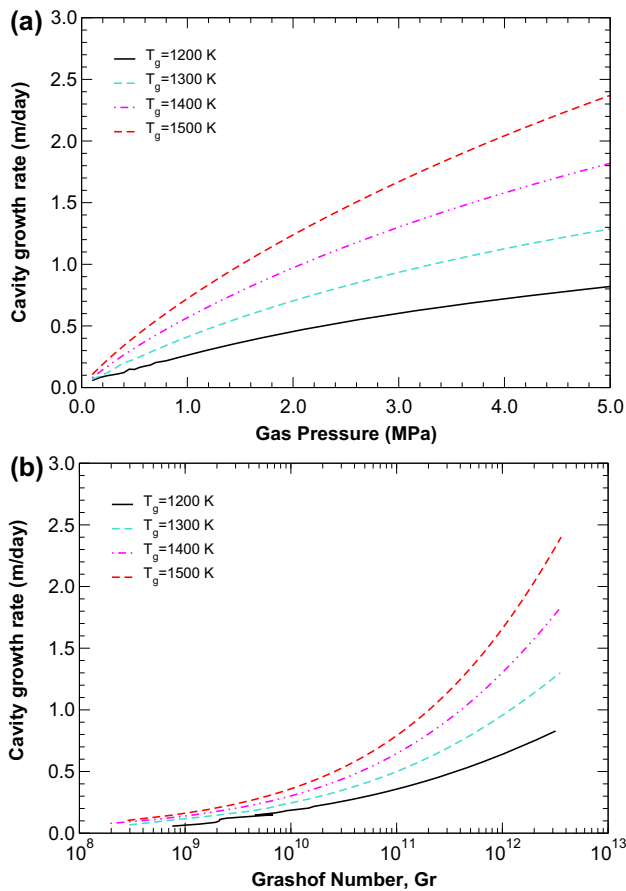

Fig. 16 Effect of gas temperature on the cavity growth rate for air and steam/oxygen gasification and two water influx rates with an ash layer thickness of $\delta_{ash} = 0.02$ m in the gasification zone

growth rate would be much lower than shown by the standalone wall submodel. For gas temperatures in the gasification zone of $1300 - 1500$ K, the cavity growth rates with a water influx of 2×10^{-3} kg/m^2 s are in the range observed in field trials, ie. $0.5 \lesssim v_c \lesssim 1.5$ m/day.

7.3 Effect of pressure

In industrial applications of UCG, the heat and mass transfer in the gasification zone which is devoid of ash is dominated by natural convection (Perkins 2018b). To study the effect of gas pressure on the cavity growth, the concentration and thermal boundary layer thicknesses are calculated using Eqs. (43)−(47). Figure 17a shows calculations of the cavity growth rate as a function of the gas pressure for gas temperatures in the range of 1200 to 1500
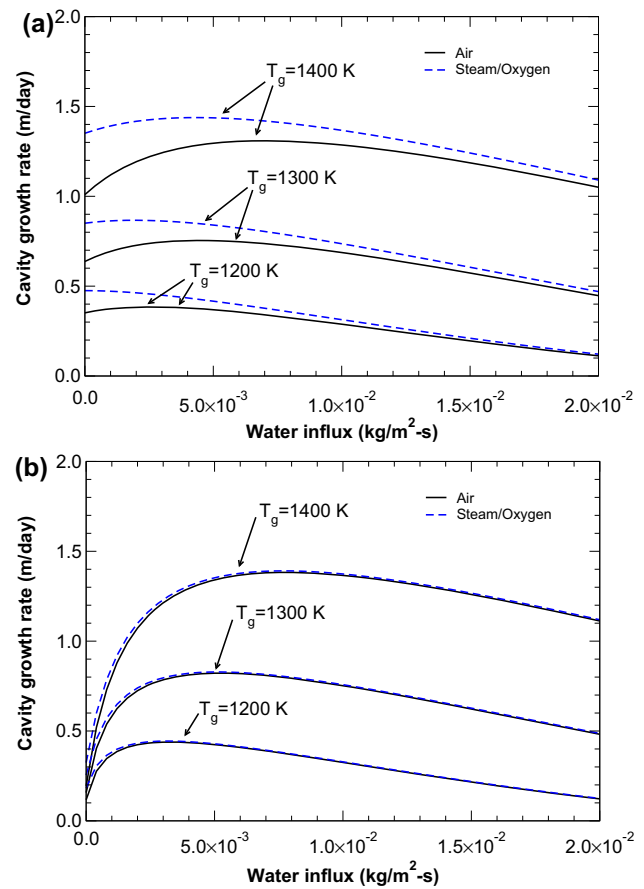
Fig. 17 Cavity growth rate during gasification with steam/oxygen and an ash layer of $\delta_{ash} = 0$ m: **a** effect of gas pressure and temperature and **b** as a function of Grashof number and gas temperature

Fig. 18 Effect of water influx and gas temperature and oxidant on cavity growth rate for: **a** $\delta_{ash} = 0$ m and **b** $\delta_{ash} = 0.02$ m

K when there is no ash layer. The corresponding plot of the data against the Grashof number is shown in Fig. 17b. It is observed that higher gas pressure leads to an increase in the cavity growth rate, primarily due to an increase in heat and mass transfer associated with higher Grashof numbers. For example at a pressure of 0.1 MPa, $Gr \sim 10^8$; while at 1 MPa $Gr \sim 3 \times 10^{10}$ at 1200 K and $Gr \sim 8 \times 10^{10}$ at 1500 K; and at 4 MPa, $Gr \sim 1 \times 10^{12}$ at 1200 K and $Gr \sim 2 \times 10^{12}$ at 1500 K.

7.4 Effect of water influx

Figure 18 shows the effect of water influx, oxidant and gas temperature on the calculated cavity growth rates in the gasification zone for two ash layer thicknesses. It is observed that average rates are significantly lower than in the combustion zone, as all energy to heat up the coal to reaction temperature and to drive the endothermic gasification reactions must be supplied via heat transfer from the bulk gas. Cavity growth rates can be increased by

supplying water, in the form of water influx, to the system. As seen in Fig. 18a when there is no ash layer present, a small amount of water influx increases the cavity growth rate by $\lesssim 30\%$, however beyond a certain level the cavity growth is reduced due to the extra energy required to evaporate water into steam. However, when an ash layer is present it severely limits the rate at which steam can be transferred from the gas to the char surface, impeding cavity growth. In this situation, the addition of water influx from the coal matrix can increase the observed cavity growth rate many times over, as shown in Fig. 18b. Under these conditions, the composition of the bulk gas has almost no influence on the cavity growth rate, as the water influx supplies almost all of the reactants for the char——steam reaction. Maximum cavity growth rates are observed with water influx rates in the range of $2 \times 10^{-3} \sim 8 \times 10^{-3}$ kg/m^2 s depending upon the temperature and ash layer thickness.
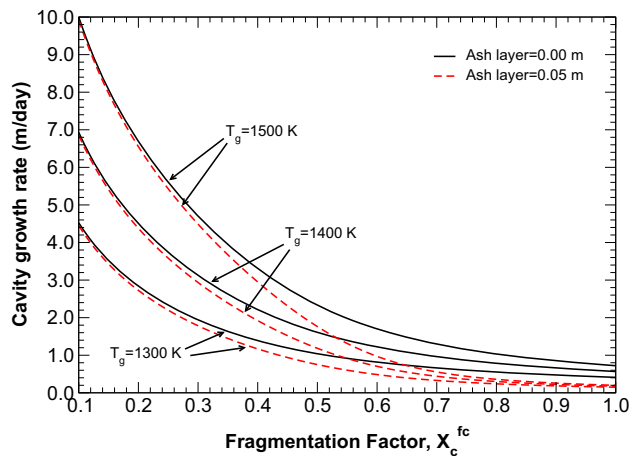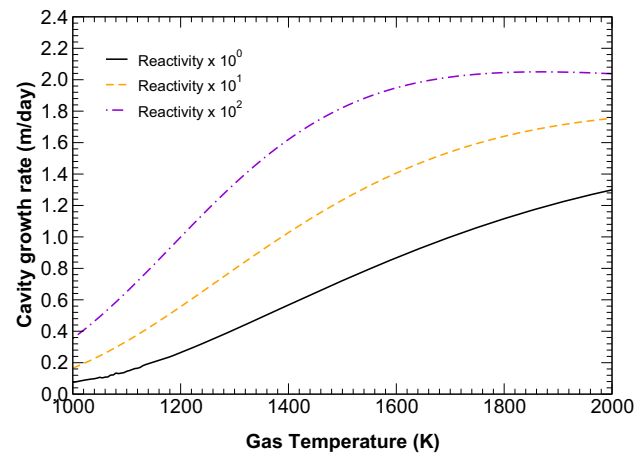
Fig. 19 Effect of coal fragmentation factor and ash layer thickness on cavity growth rate for three gas temperatures

Fig. 20 Effect of coal reactivity on cavity growth rate as a function of the bulk gas temperature

7.5 Effect of coal properties

It is known from previous work that several coal properties can have a large impact on the observed cavity growth rates. In particular, the thermo-mechanical behaviour of the coal can affect the cavity growth rates calculated by coal block gasification models (Perkins and Sahajwalla 2006). In this work, the coal fragmentation factor, X_c^{fc}, is used to represent the thermo-mechanical breakdown of the coal due to high temperatures. Figure 19 shows the effect of X_c^{fc} on the calculated cavity growth rates for three bulk gas temperatures ($T_g = 1300$, 1400 and 1500 K) and two ash layer thicknesses ($\delta_{ash} = 0$ m and $\delta_{ash} = 0.05$ m). It can be seen that the cavity growth rate increases when $X_c^{fc} < 1$ due to the spalling of unconverted fixed carbon (and associated ash) from the wall. In this situation, fixed carbon and ash particles will form a permeable bed of material at the bottom of the cavity and the fixed carbon may be subsequently combusted or gasified by the injected oxidant. While, very high cavity growth rates result from the model when a high degree of char fragmentation is assumed, in actual practice the growth rates will be tempered by heat generation and heat transfer required to induce the thermo-mechanical breakdown of the coal.

Interestingly, when $X_c^{fc} \lesssim 0.3$ the thickness of the ash layer does not significantly impact on the calculated cavity growth rate. This is because, sufficient reactants for the gasification reactions are provided by water evaporation and volatile release. When $X_c^{fc} = 1$, the cavity growth rates calculated by the model converge to ~ 0.2 m/day for all temperatures when the ash layer is thick, and between 0.4 and 0.8 m/day when there is no ash layer.

The intrinsic reactivity of the char is another coal property of interest. Figure 20 shows simulation results for the cavity growth rate as a function of gas temperature when the coal reactivity is increased 10 and 100 fold over the base case value. It can be seen that when the gas temperature is greater than ~ 1600 K and the char reactivity is high, that the growth rate becomes increasingly mass transfer limited. When the temperature is less than ~ 1200 K the cavity growth rate becomes controlled by chemical kinetics. Generally, it is expected that the gas temperature in the gasification zone will be $1200 \lesssim T_g \lesssim 1600$ K and so the coal consumption will be influenced by both mass transfer and chemical kinetics.

8 Conclusions

In this paper a 0-dimensional submodel for cavity growth in underground coal gasification has been presented. It has been demonstrated that the model can reproduce the experimental results from the laboratory combustion of coal cores and coal blocks. It has been found that the model provides good estimates of the cavity growth rates observed in field trials of underground coal gasification when reasonable assumptions of the coal properties and operating conditions are used as inputs. Simulation results of cavity growth in the combustion and gasification zones have shown the impact of key parameters such as bulk gas temperature, gas pressure, water influx, ash layer thickness, coal fragmentation and char reactivity. Importantly, the simulation outputs are consistent with detailed coal block models, while the model is sufficiently simple and robust to be incorporated into reactor scale models as a submodel for cavity growth.

References

Beath AC (1996) Mathematical modelling of entrained flow coal gasification. PhD thesis, University of Newcastle, Australia

Bird R, Stewart W, Lightfoot E (1960) Transport phenomena. Wiley, New York

Blackwood JD, McGrory F (1958) The carbon-steam reaction at high pressure. Aust J Chem 11:17–33

Bliek A, Lont JC, Swaaij WPMV (1986) Gasification of coal-derived chars in synthesis gas mixtures under intraparticle mass-transfer-controlled conditions. Chem Eng Sci 41(7):1895–1909

Boysen JE, Canfield MT, Covell JR, Schmit CR (1998) Detailed evaluation of process and environmental data from the Rocky Mountain I underground coal gasification field test. Tech. Rep. Report No. GRI-97/0331, Gas Research Institute, Chicago, IL

Britten JA (1986) Recession of a coal face exposed to a high temperature. Int J Heat Mass Transf 29(7):965–978

Britten JA, Thorsness CB (1989) A model for cavity growth and resource recovery during underground coal gasification. Situ 13(1):1–53

Cena RJ, Britten JA, Thorsness CB (1987) Excavation of the Partial Seam CRIP Underground Coal Gasification Test Site. In: Proceedings thirteenth annual underground coal gasification symposium, U.S. Department of Energy, Morgantown, WV, USA, pp 382–390, dOE/METC-88/6095

Cena RJ, Thorsness CB (1981) Underground coal gasification database. Tech. Rep. UCID-19169, Lawrence Livermore National Laboratory, University of California, Berkeley, CA, USA

Chi WK, Perlmutter DD (1989) The effect of pore structure on the char-steam reaction. AIChE J 35(11):1791–1802

Eddy TL, Schwartz SH (1983) A side wall burn model for cavity growth in underground coal gasification. J Energy Res Technol 105:145–155

Hill RW, Thorsness CB (1982) Summary report on large block experiments in underground coal gasification, Tono Basin, Washington: Vol. 1. Experimental description and data analysis. Tech. Rep. UCRL-53305, Lawrence Livermore National Laboratory, University of California, Berkeley, CA

Hill RW, Thorsness CB, Cena RJ, Stephens DR (1984) Results of the Centralia underground coal gasification field test. In: Proceedings tenth annual underground coal gasification symposium, U.S. Department of Energy, Morgantown, WV

Jiang L, Chen Z, Farouq Ali SM (2019) Heavy oil mobilization from underground coal gasification in a contiguous coal seam. Fuel 249:219–232

Kasani HA, Chalaturnyk RJ (2017) Coupled reservoir and geomechanical simulation for a deep underground coal gasification project. J Nat Gas Sci Eng 37:487–501

Kuyper RA (1994) Transport phenomena in underground coal gasification channels. PhD thesis, Delft University of Technology, The Netherlands

Levenspiel O (1972) Chemical reactor engineering, 2nd edn. Wiley, New York

Lin X, Liu Q, Liu Z, Guo X, Wang R, Shi L (2016) The role of ash layer in syngas combustion in underground coal gasification. Fuel Process Technol 143:169–175. https://doi.org/10.1016/j.fuproc.2015.12.008

Mashego A (2012) UCG Mass and energy balance methodology: Gasifier 3, Gasifier 4 and Gasifier 5. Tech. Rep. CET-UCG-REP-011, Linc Energy Ltd, Brisbane, Australia

Mashego A (2013) The evaluation of Gasifier 5 Cavity 1 to Cavity 6 performance: Gasifier 5 subsurface report. Tech. Rep. CET-UCG-REP-011, Linc Energy Ltd, Brisbane, Australia

Massaquoi JGM, Riggs JB (1983) Mathematical modeling of combustion and gasification of a wet coal slab—I model development and verification. Chem Eng Sci 38(10):1747–1756

Muhlen HJ, van Heek KH, Juntgen H (1985) Kinetic studies of steam gasification of char in the presence of H_2, CO_2 and CO. Fuel 64:944–949

Park KY, Edgar TF (1987) Modeling of early cavity growth for underground coal gasification. Ind Eng Chem Res 26:237–246

Perkins G (2018a) Underground coal gasification—Part I: field demonstrations and process performance. Prog Energy Combust Sci 67:158–187. https://doi.org/10.1016/j.pecs.2018.02.004

Perkins G (2018b) Underground coal gasification - Part II: fundamental phenomena and modeling. Prog Energy Combust Sci 67:234–274. https://doi.org/10.1016/j.pecs.2018.03.002

Perkins G, Sahajwalla V (2005) A mathematical model for the chemical reaction of a semi-infinite block of coal in underground coal gasification. Energy Fuels 19(4):1672–1692. https://doi.org/10.1021/ef0496808

Perkins G, Sahajwalla V (2006) A numerical study of the effects of operating conditions and coal properties on cavity growth in underground coal gasification. Energy Fuels 20(2):596–608. https://doi.org/10.1021/ef050242q

Perkins G, Sahajwalla V (2007) Modelling of heat and mass transport phenomena and chemical reaction in underground coal gasification. Chem Eng Res Design 85(A3):329–343. https://doi.org/10.1205/cherd06022

Perkins G, Sahajwalla V (2008) A steady-state model for estimating gas production from underground coal gasification. Energy Fuels 22(6):3902–3914. https://doi.org/10.1021/ef8001444

Perkins G, Vairakannu P (2017) Considerations for oxidant and gasifying medium selection in underground coal gasiication. Fuel Process Technol 165:145–154. https://doi.org/10.1016/j.fuproc.2017.05.010

Perkins G, du Toit E, Cochrane G, Bollaert G (2016) Overview of underground coal gasification operations at Chinchilla, Australia. Energy Sources Part A 38(24):3639–3646. https://doi.org/10.1080/15567036.2016.1188184

Poon SSK (1985) The combustion rates of Texas lignite cores. Master's thesis, The University of Texas at Austin, Austin, TX, USA

Prabu V, Jayanti S (2012) Laboratory scale studies on simulated underground coal gasification of high ash coals for carbon-neutral power generation. Energy 46:351–358. https://doi.org/10.1016/j.energy.2012.08.016

Prabu V, Jayanti S (2014) Heat-affected zone analysis of high ash coals during ex situ experimental simulation of underground coal gasification. Fuel 123:167–174. https://doi.org/10.1016/j.fuel.2014.01.035

Press WH, Teukolsky SA, Vetterling WT, Flannery BP (1992) Numerical recipes in C, 2nd edn. Cambridge University Press, Cambridge

Roberts D (2000) Intrinsic reaction kinetics of coal chars with oxygen, carbon dioxide and steam at elevated pressures. PhD thesis, University of Newcastle, Australia

Roberts DG, Harris DJ (2000) Char gasification with O_2, CO_2 and H_2O: effects of pressure on intrinsic reaction kinetics. Energy Fuels 14:483–489

Samdani G, Aghalayam P, Ganesh A, Sapru R, Lohar B, Mahajani S (2016a) A process model for underground coal gasification—

Part-I cavity growth. Fuel 181:690–703. https://doi.org/10.1016/j.fuel.2016.05.020

Samdani G, Aghalayam P, Ganesh A, Sapru R, Lohar B, Mahajani S (2016b) A process model for underground coal gasification—Part-II growth of outflow channel. Fuel 181:587–599. https://doi.org/10.1016/j.fuel.2016.05.017

Seifi M, Chen Z, Abedi J (2011) Numerical simulation of underground coal gasification using the CRIP method. Can J Chem Eng 89:1528–1535. https://doi.org/10.1002/cjce.20496

Smith IW (1978) The intrinsic reactivity of carbons to oxygen. Fuel 57:409–414

Thorsness CB, Cena RJ (1983) An Underground coal gasification cavity simulator with solid motion. Tech. Rep. UCRL-89084, Lawrence Livermore National Laboratory, University of California, Berkeley, CA, USA

Thorsness CB, Grens EA, Sherwood A (1978) A one-dimensional model for in situ coal combustion. Tech. Rep. UCRL-52523, Lawrence Livermore National Laboratory, University of California, Berkeley, CA, USA

Tomita A, Mahajan OP Jr, Walker PL Jr (1977) Reactivity of heat-treated coals in hydrogen. Fuel 56:137–144

van Batenburg D (1992) Heat and mass transfer during underground coal gasification. PhD thesis, Dietz Laboratory, Delft University of Technology, The Netherlands

Wylen GJV, Sonntag RE (1985) Fundamentals of classical thermodynamics. Wiley, New York